

Model-based Metric 3D Shape and Motion Reconstruction of Wild Bottlenose Dolphins in Drone-Shot Videos

Daniele Baieri
University of Milano-Bicocca
daniele.baieri@unimib.it

Riccardo Ciciarella
University of Zurich
riccardo.ciciarella@iea.uzh.ch

Michael Krützen
University of Zurich
michael.kruetzen@iea.uzh.ch

Emanuele Rodolà
Sapienza University of Rome
rodola@di.uniroma1.it

Silvia Zuffi
IMATI-CNR
silvia.zuffi@cnr.it

Abstract

We address the problem of estimating the metric 3D shape and motion of wild dolphins from monocular video, with the aim of assessing their body condition. While considerable progress has been made in reconstructing 3D models of terrestrial quadrupeds, aquatic animals remain unexplored due to the difficulty of observing them in their natural underwater environment. To address this, we propose a model-based approach that incorporates a transmission model to account for water-induced occlusion. We apply our method to video captured under different sea conditions. We estimate mass and volume, and compare our results to a manual 2D measurements-based method.

1. Introduction

Body size is a key morphological trait that influences physiological processes [23]. It directly affects metabolic rate, shaping energy needs, growth, reproduction, and survival [1, 22]. Additionally, it governs heat exchange efficiency [31, 32], fasting endurance [26], and movement biomechanics and energy demands [16, 18]. Body condition, a widely used body size metric, reflects an individual’s energy reserves [17, 30] and serves as a crucial indicator of population nutritional status, informing conservation and management efforts [15, 34, 37]. Traditional methods, such as direct mass measurement or morphometric proxies, provide valuable bioenergetics and health insights [8, 11, 14] but can be invasive or impractical for marine mammals [5]. Unoccupied Aerial Vehicles (UAV) photogrammetry offers a promising non-invasive alternative, enabling remote body condition and mass estimation [25, 41, 42]. However, its use has been largely limited to two-dimensional measurements, which may not fully capture body condition variabil-



Figure 1. **Data Capture.** We capture footage of dolphins in Shark Bay, Western Australia, where the clear waters allow full-body visibility from drones.

ity. Since body condition and mass are volumetric properties, incorporating three-dimensional body volume estimates could improve assessment accuracy. Motivated by this hypothesis, we address the problem of estimating the metric 3D shape and motion of dolphins from drone-shot videos captured in the wild. Then, we leverage the reconstruction to estimate mass and volume. Reconstructing the 3D pose and shape of animals from images and videos is a complex task, due to variations in appearance, non-rigid body deformations, and occlusion. Although significant progress has been made for terrestrial animals, marine species remain largely understudied. Dolphins, as highly agile aquatic mammals, present additional complexities, such as dynamic, unconstrained movement, water-induced occlusion, and the scarcity of large-scale annotated datasets. We follow a model-based optimization approach, due to the ambiguities of monocular capture and data scarcity. Specifically, we define a parametrized dolphin model, starting from a realistic template, and optimize shape and 3D pose parameters to fit video data in an analysis-by-synthesis approach, where we synthesize the textured dolphin with a model of water transmission. Model-based methods for animal [52] or human [27] 3D reconstruction are based on articulated

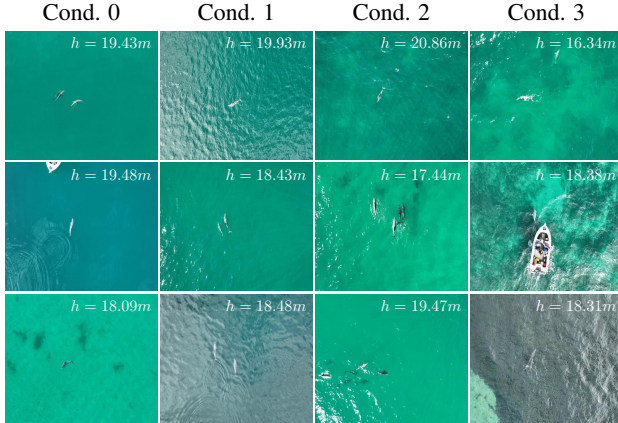


Figure 2. **Data Collection.** We show examples of frames captured under different Beaufort conditions (see Section 3.1).

parametric shape models that define low-dimensional shape deformation spaces learned from registered 3D scans. To be useful, such models should be expressive enough to represent the whole population. The low-dimensional shape model captures the correlation among all body vertices within the training set. When data is limited, this approach can make metric reconstruction difficult: *e.g.*, if the model cannot generate small individuals, size variations are compensated by placing subjects far from the camera. As we lack the possibility to scan a wide population of dolphins with comprehensive size and shape variations, we define a 3D parametric model via per-part synthetic shape deformation spaces, including uniform and anisotropic part scaling, similarly to the GLOSS model [52]. This approach has the advantage of breaking the whole-body correlations, allowing to generate a wide range of shapes. Note that previous work has adopted bone scaling [2, 3], but this would not suffice in our case, as we seek to estimate body volume. In our experiments, we obtain 3D shape and motion for videos captured under varying sea conditions, and compute the mass and volume of the estimated 3D dolphins. To our knowledge, we are the first to address the problem of 3D reconstruction of dolphins from monocular video for mass and volume estimation, and to incorporate a water occlusion model into a framework for the 3D reconstruction of animals.

2. Related Work

While significant progress has been made in model-based 3D human pose and shape estimation, extending these methodologies to animals presents unique challenges. These include creating suitable 3D parametric shape models that account for inter- and intra-species variations and capturing large datasets with ground-truth 3D pose and shape annotations. A significant body of work has focused on

quadrupeds [3, 24, 29, 35, 36] and birds [2, 40], yet less attention has been devoted to estimating the 3D pose and shape of aquatic animals such as dolphins. Cashman and Fitzgibbon [4] were the first to address the 3D reconstruction of dolphins from images. Irschick et al. [19] create 3D models of dolphins using photogrammetry. Zuffi et al. [52] introduced SMAL, the first multi-species model analogous to the SMPL model of the human body [27]. Alternative (model-free) approaches aim to reconstruct animals without a 3D parametric shape model [20, 43–51]. While these methods are theoretically more general, they often produce unsatisfactory results, require multi-view data, or depend on category-based datasets for learning shape.

3. Method

We solve our problem as an instance of single-view inverse rendering. Our pipeline requires a single drone-shot video of a dolphin with T frames, labeled with the altitude values of the camera $\{h_i\}_{i=1}^T$. The two core parts of our method are 1) a SMPL-like [27, 28] dolphin template model, supporting differentiable skinning and part scaling, and 2) the DIB-R [6, 7] differentiable mesh rendering algorithm.

3.1. Data Collection

We collected aerial videos in 2024 from a population of Indo-Pacific bottlenose dolphins (*Tursiops aduncus*) in Shark Bay, Western Australia. We used a Mavic 3 multi-rotor UAV (DJI), equipped with a CMOS four-thirds camera (20 effective megapixels; Hasselblad) with a 24 mm f/2.8 to f/11 lens. The drone was equipped with a SF11/C laser range finder (LightWare LiDAR) to measure the altitude above the focal animals. We operated the drone at altitudes of 15 – 25 m from the water surface. When recording the dolphins, we angled the cameras of the drone vertically at -90° (zenithal angle), and used a video resolution of 5.1K@50fps. We conducted UAV flights in favorable conditions, limiting operations to Beaufort 0–3 conditions. At Beaufort 0, the water was mirror-like; at Beaufort 1, slight ripples formed without foam crests. Beaufort 2 produced small wavelets with occasional crests, while Beaufort 3 introduced short waves with scattered whitecaps, though visibility remained sufficient (see Fig. 2).

Using the same drone setup as in the field, we collected in 2023 morphometric data on 11 Indo-Pacific (*T. aduncus*) and 14 common (*T. truncatus*) bottlenose dolphins under professional human care at Sea World in Gold Coast, Queensland, Australia. We captured video recordings of both the dorsal and lateral perspective of the dolphins while they remained stationary in the shallow-water section of the pool, assisted by the trainers. For lateral recordings, trainers guided the dolphins to rotate their bodies in the water, allowing imaging from the left or right side. From the dorsal images, we determined body length (BL, measured from the

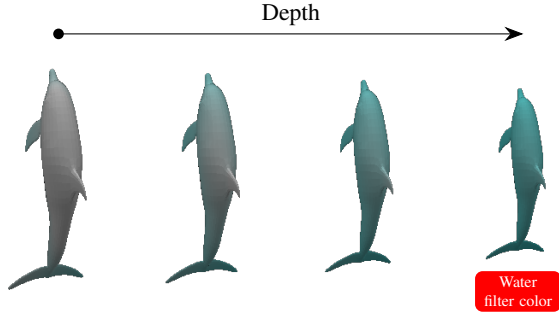


Figure 3. **Water filtering.** We show the effect of our water filter, with a fixed color (bottom right), by varying the distance of the dolphin mesh from the water plane.

rostrum tip to the end of the tail notch) and body widths (W) at 5% increments along the body axis [8, 9]. Similarly, lateral images were used to assess body height (H , the dorso-ventral distance) at the same measurement locations as the width assessments [10]. In total, we obtained 19 W and H measurements, which were analyzed using MorphoMetrix software [38].

3.2. 3D Reconstruction

3.2.1. Preprocessing

Inferring 3D information from single-view images is a notoriously hard problem. In order to make it feasible without simplifying assumptions, we need to inject priors into the model. First, we segment the target dolphin in the input videos using the SAM-2 model [33]. Thanks to its excellent tracking abilities, SAM-2 provides reasonable masks in most cases, even when the dolphins would dive deep and gradually disappear. Then, we employ this information to initialize the position of the dolphin for all frames: by exploiting the fact that all images are perpendicular drone shots with known altitude, we can map the center of the dolphin geometry in world space to the center of the masked pixels in image space by inverting the camera transform.

3.2.2. Model

We model various features of the scene depicted in the input videos, in order to ensure the most accurate reconstruction of the dolphin geometry.

Articulated dolphin model Similarly to [52], we create a parametric shape model given a dolphin template segmented into body parts, with synthetic deformation spaces defined for each part. The dolphin model follows a representation similar to 3D parametric shape models of humans and animals, computing the vertices of a triangular mesh given pose and shape parameters. The model is a function $M(\beta, \vartheta)$ of shape β and pose ϑ . β is the matrix of shape variables, while $\vartheta \in \mathbb{R}^{3 \times N}$ is the relative rotation,

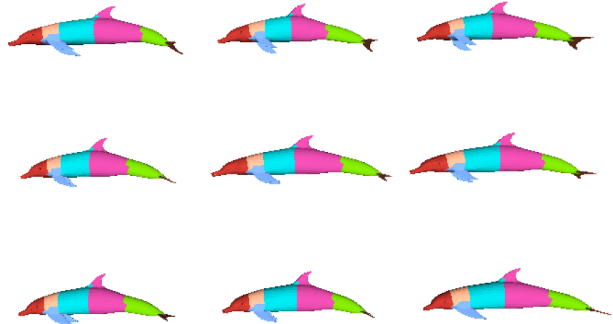


Figure 4. **Samples.** We show samples from the dolphin model; note how we can create different shapes by deforming the body parts.

expressed with Rodrigues vectors, of the N joints in the kinematic tree. Differently from previous models, the shape variables in the dolphin model are a matrix rather than a vector, as we have a vector of shape variables for each body part. The model computes the coordinates of the vertices in the template pose for each body part as:

$$\mathbf{v}_{\text{shape}, J_i}(\beta_i) = \mathbf{v}_{t, J_i} + B_{J_i} \beta_i, \quad (1)$$

where \mathbf{v}_t represents the vertices of the dolphin template, B is a matrix of deformation vectors, β_i is the shape vector corresponding to the part i . J_i is the set of vertex indices that belong to the part i . Given vertices of different parts are independently modified, the resulting model is not smoothly connected at the part skin interfaces. Joint displacements are computed to connect each part to its parent in the kinematic tree. The matrix of shape components B is defined as the synthetic shape space of the GLoSS model [52]. Samples from the model are shown in Fig. 4.

Scene model We group our joints into $M \leq N$ parts, allowing to account for symmetries in motion and scale (e.g., fins, flukes). We control these for optimization via pose parameters $\theta \in \mathbb{R}^{T \times M \times 3}$ and (non-time dependent) shape parameters $\beta \in \mathbb{R}^{M \times 4}$. The first group/joint represents the root bone, i.e., it controls the global orientation of the dolphin. The position of the dolphin, on the other hand, is modeled as a per-frame translation of the root bone $\mathbf{P} \in \mathbb{R}^{T \times 3}$. The model comes with UV maps, which allows us to represent its appearance via a color texture $I_{\text{albedo}} \in [0; 1]^{H_a \times W_a}$. We made it grayscale to prevent water effects from bleeding into the dolphin appearance during optimization. We then modeled such effects separately by introducing a novel water filter. After obtaining a render $C \in [0; 1]^{H_r \times W_r \times 3}$ of the scene, we post-process it as:

$$\hat{C}_{i,j} = C_{i,j} \circ \exp(\min(d_{i,j}, 0) \cdot F_{\text{water}}), \quad (2)$$

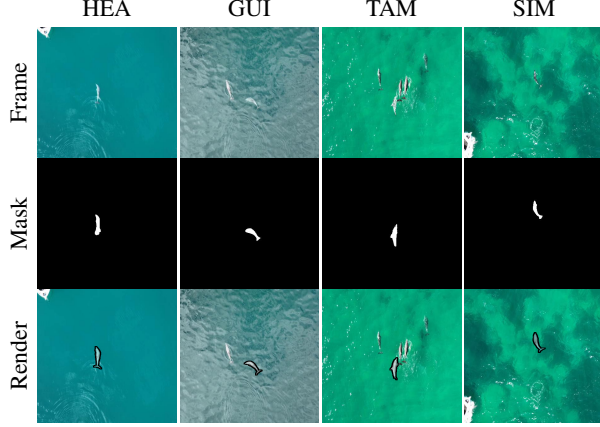


Figure 5. **Image reconstruction.** For 4 scenes in our dataset, we show (from top to bottom) the original video frame, the SAM-2 segmentation, and the rendering obtained after optimization.

where $F_{\text{water}} \in [0; 1]^3$ is a parameter modeling which color frequencies are filtered by a volume of water, and $d_{i,j}$ is the (negative) depth of the dolphin at pixel (i, j) . This information is available via the camera altitude, which allows us to assume that the water plane lies at 0 along the up axis of the scene. Lastly, illumination effects are captured by a simple spherical Gaussians [39] model with parameters S . Summarizing, the scene parameters for optimization are $\Theta = \{\theta, \beta, P, I_{\text{albedo}}, F_{\text{water}}, S\}$.

3.2.3. Optimization

Additional to the altitude and pose, we employ the intrinsic properties of the drone camera to ensure correspondence in length units between virtual and real space. Using the sensor width γ and focal length ω , the field of view of the virtual camera is defined as $\text{fov} = 2 \cdot \tan^{-1} \left(\frac{\gamma}{2\omega} \right)$. The base dolphin model is rescaled so that its initial length fits 2.6m, which is the average length for the species of dolphin depicted in our data. The loss function we use to optimize our scene is defined as the sum of multiple terms, which we describe in the following paragraphs. The loss function is optimized iteratively via Adam [21] steps.

Reconstruction losses Our data fidelity terms follow common choices from past literature. Given the complete render of the current scene model $\hat{C}^{(t)}$ at frame t , the corresponding ground truth image $I^{(t)}$ and the mask $B \in \{0, 1\}^{H_r \times W_r}$ specifying which pixels were mapped to the dolphin mesh during rendering, we compute the photometric loss as:

$$L_{\text{RGB}} = \sum_{i=1}^{H_r} \sum_{j=1}^{W_r} \left\| B_{i,j} \cdot \left(\hat{C}_{i,j}^{(t)} - I_{i,j}^{(t)} \right) \right\|_2^2 \quad (3)$$

Given the output DIB-R soft mask $\hat{B}^{(t)}$ at frame t , we

optimize the dolphin shape with respect to the SAM-2 segmentation mask \bar{B} using an Intersection-over-Union loss:

$$L_{\text{mask}} = 1 - \sum_{i=1}^{H_r} \sum_{j=1}^{W_r} \frac{\hat{B}_{i,j}^{(t)} \bar{B}_{i,j}^{(t)}}{\left(\hat{B}_{i,j}^{(t)} + \bar{B}_{i,j}^{(t)} \right) - \hat{B}_{i,j}^{(t)} \bar{B}_{i,j}^{(t)}} \quad (4)$$

Distribution terms To avoid obtaining degenerate behaviour with out-of-distribution values in the pose or scale parameters, we regularize both to have minimal L2 norm (*i.e.*, values close to zero) via the L_{pose} and L_{scale} terms:

$$L_{\text{pose}} = \|\theta\|_2^2, \quad L_{\text{scale}} = \|\beta\|_2^2 \quad (5)$$

Scale regularizers Given that one dimension of the dolphin is frequently unobserved in the data, we want to avoid its scale value being completely independent from the dolphin’s size in the other dimensions. To this end, we penalize differences in scale for distinct axes of the same group:

$$L_{\text{scale}}^{\text{axes}} = \sum_{k=1}^M \left(\|\beta_{k,2} - \beta_{k,3}\|_2^2 + \|\beta_{k,2} - \beta_{k,4}\|_2^2 + \|\beta_{k,3} - \beta_{k,4}\|_2^2 \right) \quad (6)$$

The first scale component of each group is the global scale, therefore we do not consider it in this regularizer.

Then, to avoid large variations of scale in adjacent model parts, we employ the model skeleton’s structure to penalize differences in the scale of the k -th bone group and its parent $p(k)$:

$$L_{\text{scale}}^{\text{smooth}} = \sum_{k=2}^M \left\| \beta_k - \beta_{p(k)} \right\|_2^2 \quad (7)$$

We skip the first group as the root bone has no parent.

Smoothness terms We regularize the variation over time of per-frame parameters (dolphin position, orientation and joints pose) by minimizing the MSE between their values at adjacent frames. In practice, fitting the terms $L_{\text{smooth}}^{\text{pos}}$, $L_{\text{smooth}}^{\text{rot}}$, and $L_{\text{smooth}}^{\text{joints}}$ along with our reconstruction losses allows us to obtain smooth animations. The regularization for the root bone’s pose is computed separately from that of the other bone groups, since we observed that different loss weights between the global orientation smoothness term and the joints pose smoothness term could be beneficial.

$$L_{\text{smooth}}^{\text{pos}} = \sum_{t=2}^T \left\| P_t - P_{t-1} \right\|_2^2 \quad (8)$$

$$L_{\text{smooth}}^{\text{rot}} = \sum_{t=2}^T \left\| \theta_{t,1} - \theta_{t-1,1} \right\|_2^2 \quad (9)$$

$$L_{\text{smooth}}^{\text{joints}} = \sum_{t=2}^T \sum_{j=2}^M \left\| \theta_{t,j} - \theta_{t-1,j} \right\|_2^2 \quad (10)$$

Direction term In scenes where the dolphin moves independently of the drone’s movement, we want to ensure that it actually moves in its forward direction. We penalize inconsistent behaviour with the cosine distance between the dolphin’s forward vector and the normalized change in position (L_{dir}). Given z the forward vector of the dolphin in rest pose, we define this loss as

$$L_{\text{dir}} = \sum_{t=2}^T 1 - \left(R_{\theta_{t,1}}(z) \cdot \frac{P_t - P_{t-1}}{\|P_t - P_{t-1}\|} \right) \quad (11)$$

where $R_{\theta}(x)$ applies the 3D rotation with axis angles θ to the 3D vector x . We omit the denominator from the cosine similarity, as both vectors have norm 1. When the drone accurately tracks the dolphin (which is often the case), its position should not change and we disable this term. Additionally, due to the vertical motion being unobservable from a drone shot, we adjust the vertical position of the dolphin depending on its orientation. For each frame that the dolphin points upwards, we increase its vertical position by v_{surf} m/s , while we decrease it by v_{dive} m/s when it points downwards.

4. Evaluation

In this section, we present our method’s evaluation in comparison with a measurement-based baseline. The values of hyperparameters used in our experiments may be found in the supplementary materials. For all experiments, the model is optimized for 100 epochs, requiring ~ 20 min per 10 seconds of video on a NVIDIA RTX 4060Ti GPU.

We provide the values of hyperparameters used in our experiments in Table 1. Each loss term L_* has an associated weight λ_* used during aggregation. The table is split into the following groups: rendering parameters, loss weights, optimization parameters, and others. The parameters $\frac{1}{\sigma}$, box length and k are not mentioned in the main text, as these are DIB-R parameters which influence how the soft mask is computed. In the optimization group, we split the learning rate (LR) for categories of parameters as we empirically observed benefits in doing so, possibly due to the difference in range of values for color parameters vs transform parameters.

4.1. Baseline

To evaluate our method, we implemented a baseline for computing body volume and mass, adapting previous work by Christiansen et al. [10]. The resulting Elliptical Volume Estimation method estimates volume by approximating the animal body with a set of elliptical segments. These segments are obtained by manually annotating selected frames of the videos and then applying a model of width-height ratio learned from animals in captivity. Applying this baseline to wild animals could, therefore, result in a bias.

	Parameter	Value
Rendering	$\frac{1}{\sigma}$	100000
	Box length	0.01
	k	40
	γ	17.27 [mm]
	ω	12.29 [mm]
	(H_r, W_r)	(720, 480)
	(H_a, W_a)	(512, 512)
Loss weights	L_{RGB}	1.0
	L_{mask}	1.0
	L_{pose}	1.0
	L_{scale}	0.005
	$L_{\text{scale}}^{\text{axes}}$	1.0
	$L_{\text{scale}}^{\text{smooth}}$	200.0
	$L_{\text{smooth}}^{\text{pos}}$	500.0
	$L_{\text{smooth}}^{\text{rot}}$	500.0
	$L_{\text{smooth}}^{\text{pose}}$	500.0
	$L_{\text{dir}} (*)$	0.1
Optimization	Epochs	100
	LR - θ	0.01
	LR - β, P	0.01
	LR - $I_{\text{albedo}}, F_{\text{water}}$	0.001
	LR - S	0.01
Misc	v_{surf}	6.6 [m/s]
	v_{dive}	2.2 [m/s]

Table 1. Hyperparameter values employed in the experiments described in the main paper. (*): optional parameter, was set to 0 whenever not useful.

At each 5% measurement site along the body, we calculated the height-to-width (HW) ratio for each dolphin under professional care [10]. Body volume (BV) was then estimated using the segmented elliptical model described by Christiansen et al. [10]:

$$V_{(s,i)} = BL_i \times 0.05 \times \int_0^1 \frac{\pi \times (W_{A,s,i} + (W_{P,s,i} - W_{A,s,i}) \times x)}{2} \times \frac{(H_{A,s,i} + (H_{P,s,i} - H_{A,s,i}))}{2} dx \quad (12)$$

$$BV_{\text{obs},i} = \sum_{s=1}^{20} V_{s,i} \quad (13)$$

Here $V_{s,i}$ represents the volume of segment s (total of 20) for individual i , where BL_i as body length, and anterior/posterior width ($W_{A,s,i}$, $W_{P,s,i}$) and height ($H_{A,s,i}$,

ID	Cond.	Volume (m^3)		Mass (kg)	
		Ellip.	3D	Ellip.	3D
CLL	0	0.122	0.164	120.55	162.28
SLK	0	0.111	0.149	110.70	148.82
ELM	0	0.107	0.189	111.59	197.54
HEA	0	0.144	0.220	140.19	215.26
GRE	1	0.124	0.196	126.17	199.87
ESK	1	0.116	0.162	114.35	159.87
GUI	1	0.104	0.216	106.98	222.67
BUC	1	0.117	0.182	114.94	178.39
SMU	2	0.146	0.185	142.96	181.48
POO	2	0.136	0.220	132.11	213.82
WIM	2	0.121	0.164	121.41	163.69
TAM	2	0.118	0.149	114.74	144.86
WIN	3	0.116	0.221	128.44	222.82
SNR	3	0.120	0.180	118.49	177.05
LAT	3	0.130	0.154	125.53	153.89
SIM	3	0.128	0.160	127.34	158.53

Table 2. **Volume and Mass Estimate.** We report the volume and mass estimate for 16 subjects across 4 different Beaufort conditions. We compare the quantities obtained with the Elliptical method with those obtained from the 3D model. Details about the mass estimation and a plot visualization of the results are given in the supplementary material.

$H_{P,s,i}$) measurements. The integral calculates the elliptical cross-sectional area ($A = \pi \times r_1 \times r_2$) where r_1 are the major and minor radii [10]. To account for body tapering towards the tail and rostrum, W and H were set to zero at body endpoints (0% and 100% BL). Values at 90% and 95% BL were linearly interpolated from 85% and 100% BL [10]. The total observed body volume ($BV_{(obs,i)}$) for each individual was obtained by summing the volumes of the 20 segments calculated using the first equation. For wild dolphins, BL and W at the 19 measurement sites were obtained from UAV footage. Since direct H measurements are rarely feasible, H was predicted from the W using the mean HW ratio at each site [12–14].

4.2. Mass Estimation

Body condition We estimated the body condition index (BCI) using the approach described by Christiansen et al. [9]:

$$BCI_i = \frac{BV_{obs,i} - BV_{exp,i}}{BV_{exp,i}} \quad (14)$$

where $BV_{obs,i}$ (m^3) represents the measured body volume of dolphin i , and $BV_{exp,i}$ (m^3) is the expected body volume based on the log-log linear relationship between body volume and body length.

Body mass and density We calculate the dolphins’ body mass by multiplying body volume (BV) by body density

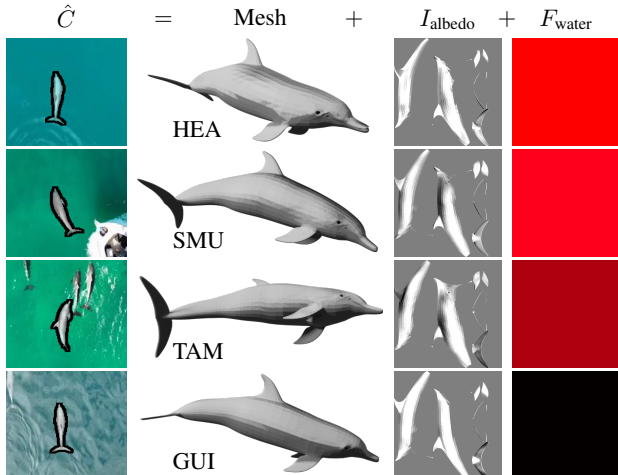


Figure 6. **3D reconstruction.** Given 4 scenes in our dataset, we show the rendering in a selected frame after optimization, along with the components used for computing it: the dolphin’s shape (including localization), its albedo texture, and the water filter.

(BD), which is determined by dividing the body mass measured from the dolphins under professional care by their estimated BV. We examined the relationship between BD and body condition index (BCI) using linear regression models. Given that cetaceans store energy primarily as blubber, which is less dense than muscle, we hypothesized a negative BD-BCI relationship:

$$BD_i = \alpha - \beta \times BCI_i \quad (15)$$

The predicted body mass (BM) was then calculated as:

$$BM_{Pred} = BV_{obs} \times BD \quad (16)$$

$$BM_{Pred} = BV_{obs} \times \left(\alpha - \beta \times \frac{BV_{obs,i} - BV_{exp,i}}{BV_{exp,i}} \right) \quad (17)$$

We illustrate the results obtained with the Elliptical Volume estimation method and with the 3D model in Fig. 7.

4.3. Discussion

Figure 5 shows renderings of the optimized scene at a selection of frames for multiple scenes in our dataset. These results portray the model’s ability of matching the the scene’s parameters to the observed mask and color. Nonetheless, the intrinsic under-determination of monocular 3D reconstruction may lead to results such as HEA: while the dolphin shape correctly overlaps with the mask, its pose differs from that showed in the image. In Figure 6, on the other hand, we aim to isolate the individual components of our scene model: thus, for each rendered frame, we show the corresponding dolphin geometry, albedo, and water filter. It is

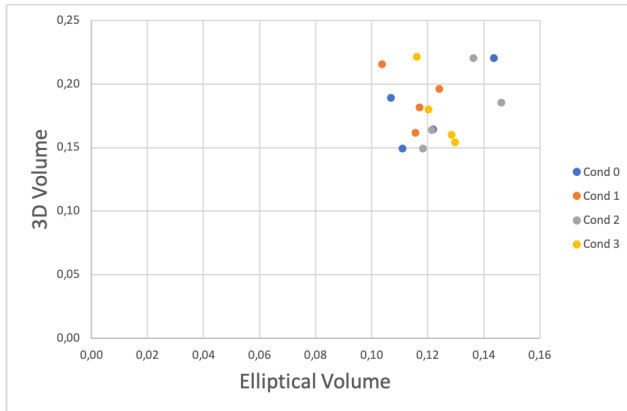


Figure 7. **Results.** We report the results obtained by measuring volume with the 3D body model and the Elliptical Volume method. Different colors indicate different Beaufort conditions (see main text).

interesting to observe that, in the GUI scene, the high transparency in the water results in a near-black filter (very weak filtering with increasing depth). Lastly, we note that most textures present baked shadows, an artifact which could be resolved with a more sophisticated lighting model. A quantitative evaluation of our method is presented in Table 2: first, we note that in most cases we observe a good correlation with the elliptical method, with our method generally providing larger volume estimates. However, after computing the mass from our volume estimate, we always achieve reasonable values for the studied species (below 230kg).

5. Conclusion

Our work represents the first investigation of metric 3D reconstruction of dolphins from monocular video to assess body condition. Future work includes accounting for visual distortions caused by water refraction and collecting a novel dataset of captured dolphins with known mass and volume for validation.

Acknowledgements. SZ is supported by PNRR FAIR Future AI Research (PE00000013), Spoke 8 Pervasive AI (CUP H97G22000210007) and NBFC National Biodiversity Future Center (CN00000033), Spoke 4 (CUP B83C22002930006) under the NRRP MUR program by NextGenerationEU.

References

- [1] Kristina J Anderson-Teixeira, Van M Savage, Andrew P Allen, and James F Gillooly. Allometry and metabolic scaling in ecology. *Encyclopedia of life sciences*, 1(10), 2009. 1
- [2] Marc Badger, Yufu Wang, Adarsh Modh, Ammon Perkes, Nikos Kolotouros, Bernd Pfrommer, Marc Schmidt, and Kostas Daniilidis. 3D bird reconstruction: a dataset, model, and shape recovery from a single view. In *ECCV*, pages 1–17, 2020. 2
- [3] Benjamin Biggs, Oliver Boyne, James Charles, Andrew Fitzgibbon, and Roberto Cipolla. Who left the dogs out? 3D animal reconstruction with expectation maximization in the loop. In *ECCV*. Springer, 2020. 2
- [4] T. J. Cashman and A. W. Fitzgibbon. What shape are dolphins? building 3D morphable models from 2d images. *IEEE Transactions on Pattern Analysis and Machine Intelligence*, 35(1):232–244, 2013. 2
- [5] J Castrillon and SB Nash. Evaluating cetacean body condition; a review of traditional approaches and new developments. *ecol evol* 10: 6144–6162, 2020. 1
- [6] Wenzheng Chen, Jun Gao, Huan Ling, Edward J. Smith, Jaakko Lehtinen, Alec Jacobson, and Sanja Fidler. *Learning to predict 3D objects with an interpolation-based differentiable renderer*. Curran Associates Inc., Red Hook, NY, USA, 2019. 2
- [7] Wenzheng Chen, Joey Litalien, Jun Gao, Zian Wang, Clement Fuji Tsang, Sameh Khalis, Or Litany, and Sanja Fidler. DIB-R++: Learning to predict lighting and material with a hybrid differentiable renderer. In *Advances in Neural Information Processing Systems (NeurIPS)*, 2021. 2
- [8] Fredrik Christiansen, Antoine M Dujon, Kate R Sprogis, John PY Arnould, and Lars Bejder. Noninvasive unmanned aerial vehicle provides estimates of the energetic cost of reproduction in humpback whales. *Ecosphere*, 7(10):e01468, 2016. 1, 3
- [9] Fredrik Christiansen, Fabien Vivier, Claire Charlton, Rhianne Ward, Alicia Amerson, Stephen Burnell, and Lars Bejder. Maternal body size and condition determine calf growth rates in southern right whales. *Marine Ecology Progress Series*, 592:267–281, 2018. 3, 6
- [10] Fredrik Christiansen, Mariano Sironi, Michael J Moore, Matías Di Martino, Marcos Ricciardi, Hunter A Warick, Duncan J Irschick, Robert Gutierrez, and Marcela M Uhart. Estimating body mass of free-living whales using aerial photogrammetry and 3d volumetrics. *Methods in Ecology and Evolution*, 10(12):2034–2044, 2019. 3, 5, 6
- [11] Fredrik Christiansen, Stephen M Dawson, John W Durban, Holly Fearnbach, Carolyn A Miller, Lars Bejder, Marcela Uhart, Mariano Sironi, Peter Corkeron, William Rayment, et al. Population comparison of right whale body condition reveals poor state of the north atlantic right whale. *Marine Ecology Progress Series*, 640:1–16, 2020. 1
- [12] Fredrik Christiansen, Kate R Sprogis, Jasmin Gross, Juliana Castrillon, Hunter A Warick, Eva Leunissen, and Susan Bengtson Nash. Variation in outer blubber lipid concentration does not reflect morphological body condition in humpback whales. *Journal of Experimental Biology*, 223(8): jeb213769, 2020. 6
- [13] Fredrik Christiansen, Fabian Rodríguez-González, Sergio Martínez-Aguilar, Jorge Urbán, Steven Swartz, Hunter Warick, Fabien Vivier, and Lars Bejder. Poor body condition associated with an unusual mortality event in gray whales. *Marine Ecology Progress Series*, 658:237–252, 2021.
- [14] Fredrik Christiansen, Outi M Tervo, Mads Peter Heide-Jørgensen, and Jonas Teilmann. Prey consumption of bow-

- head whales in west greenland estimated from drone measurements of body size and condition. *Polar Biology*, 47(1): 17–39, 2024. 1, 6
- [15] F Stephen Dobson. Body mass, structural size, and life-history patterns of the columbian ground squirrel. *The American Naturalist*, 140(1):109–125, 1992. 1
- [16] Theodore Garland Jr. Scaling the ecological cost of transport to body mass in terrestrial mammals. *The American Naturalist*, 121(4):571–587, 1983. 1
- [17] John Hanks. Characterization of population condition. *Dynamics of large mammal populations*, 1981. 1
- [18] Duncan J Irschick and Timothy E Higham. *Animal athletes: an ecological and evolutionary approach*. Oxford University Press, 2016. 1
- [19] Duncan J. Irschick, Johnson Martin, Ursula Siebert, Jakob H. Kristensen, Peter T. Madsen, and Fredrik Christiansen. Creation of accurate 3d models of harbor porpoises (*phocoena phocoena*) using 3d photogrammetry. *Marine Mammal Science*, 37(2):482–491, 2021. 2
- [20] Angjoo Kanazawa, Shubham Tulsiani, Alexei A. Efros, and Jitendra Malik. Learning category-specific mesh reconstruction from image collections. In *ECCV*, 2018. 2
- [21] Diederik P. Kingma and Jimmy Ba. Adam: A method for stochastic optimization. *CoRR*, abs/1412.6980, 2014. 4
- [22] Max Kleiber. Body size and metabolic rate. *Physiological reviews*, 27(4):511–541, 1947. 1
- [23] George V Lauder. Form and function: structural analysis in evolutionary morphology. *Paleobiology*, 7(4):430–442, 1981. 1
- [24] Ci Li, Yi Yang, Zehang Weng, Elin Hernlund, Silvia Zuffi, and Hedvig Kjellström. Dessie: Disentanglement for articulated 3d horse shape and pose estimation from images. In *Asian Conference on Computer Vision*, 2024. 2
- [25] Julie Linchant, Jonathan Lisein, Jean Semeki, Philippe Lejeune, and Cédric Vermeulen. Are unmanned aircraft systems (uas s) the future of wildlife monitoring? a review of accomplishments and challenges. *Mammal review*, 45(4):239–252, 2015. 1
- [26] Stan L Lindstedt and Mark S Boyce. Seasonality, fasting endurance, and body size in mammals. *The American Naturalist*, 125(6):873–878, 1985. 1
- [27] Matthew Loper, Naureen Mahmood, Javier Romero, Gerard Pons-Moll, and Michael J. Black. Smpl: a skinned multi-person linear model. *ACM Trans. Graph.*, 34(6), 2015. 1, 2
- [28] Matthew Loper, Naureen Mahmood, Javier Romero, Gerard Pons-Moll, and Michael J. Black. *SMPL: A Skinned Multi-Person Linear Model*. Association for Computing Machinery, New York, NY, USA, 1 edition, 2023. 2
- [29] Jin Lyu, Tianyi Zhu, Yi Gu, Li Lin, Pujin Cheng, Yebin Liu, Xiaoying Tang, and Liang An. Animer: Animal pose and shape estimation using family aware transformer, 2024. 2
- [30] JS Millar and GJ Hickling. Fasting endurance and the evolution of mammalian body size. *Functional Ecology*, pages 5–12, 1990. 1
- [31] Polly K Phillips and James E Heath. Dependency of surface temperature regulation on body size in terrestrial mammals. *Journal of Thermal Biology*, 20(3):281–289, 1995. 1
- [32] Warren P Porter and Michael Kearney. Size, shape, and the thermal niche of endotherms. *Proceedings of the National Academy of Sciences*, 106(supplement_2):19666–19672, 2009. 1
- [33] Nikhila Ravi, Valentin Gabeur, Yuan-Ting Hu, Ronghang Hu, Chaitanya Ryali, Tengyu Ma, Haitham Khedr, Roman Rädle, Chloe Rolland, Laura Gustafson, Eric Mintun, Junting Pan, Kalyan Vasudev Alwala, Nicolas Carion, Chao-Yuan Wu, Ross Girshick, Piotr Dollar, and Christoph Feichtenhofer. SAM 2: Segment anything in images and videos. In *The Thirteenth International Conference on Learning Representations*, 2025. 3
- [34] Rosalind M Rolland, Robert S Schick, Heather M Pettis, Amy R Knowlton, Philip K Hamilton, James S Clark, and Scott D Kraus. Health of north atlantic right whales eubalaena glacialis over three decades: from individual health to demographic and population health trends. *Marine Ecology Progress Series*, 542:265–282, 2016. 1
- [35] Nadine Rueegg, Silvia Zuffi, Konrad Schindler, and Michael J. Black. BARC: Learning to regress 3D dog shape from images by exploiting breed information. In *CVPR*, pages 3876–3884, 2022. 2
- [36] Nadine Ruegg, Shashank Tripathi, Konrad Schindler, Michael J. Black, and Silvia Zuffi. BITE: Beyond priors for improved three-D dog pose estimation. In *CVPR*, pages 8867–8876, 2023. 2
- [37] RD Stevenson and William A Woods Jr. Condition indices for conservation: new uses for evolving tools. *Integrative and comparative biology*, 46(6):1169–1190, 2006. 1
- [38] Walter I Torres and KC Bierlich. Morphometrix: a photogrammetric measurement gui for morphometric analysis of megafauna. *Journal of Open Source Software*, 5(45):1825, 2020. 3
- [39] Jiaping Wang, Peiran Ren, Minmin Gong, John Snyder, and Baining Guo. All-frequency rendering of dynamic, spatially-varying reflectance. *ACM Trans. Graph.*, 28(5):1–10, 2009. 4
- [40] Yufu Wang, Nikos Kolotouros, Kostas Daniilidis, and Marc Badger. Birds of a feather: Capturing avian shape models from images. In *CVPR*, pages 14739–14749, 2021. 2
- [41] Adam C Watts, John H Perry, Scot E Smith, Matthew A Burgess, Benjamin E Wilkinson, Zoltan Szantoi, Peter G Ifju, and H Franklin Percival. Small unmanned aircraft systems for low-altitude aerial surveys. *The Journal of Wildlife Management*, 74(7):1614–1619, 2010. 1
- [42] Ken Whitehead, Chris H Hugenholtz, Stephen Myshak, Owen Brown, Adam LeClair, Aaron Tamminga, Thomas E Barchyn, Brian Moorman, and Brett Eaton. Remote sensing of the environment with small unmanned aircraft systems (uass), part 2: scientific and commercial applications. *Journal of unmanned vehicle systems*, 2(3):86–102, 2014. 1
- [43] Shangzhe Wu, Tomas Jakab, Christian Rupperecht, and Andrea Vedaldi. DOVE: Learning deformable 3D objects by watching videos. *International Journal of Computer Vision (IJCV)*, 2023. 2
- [44] Shangzhe Wu, Ruining Li, Tomas Jakab, Christian Rupperecht, and Andrea Vedaldi. MagicPony: Learning articulated 3D animals in the wild. In *CVPR*, 2023.

- [45] Gengshan Yang, Deqing Sun, Varun Jampani, Daniel Vlasic, Forrester Cole, Huiwen Chang, Deva Ramanan, William T Freeman, and Ce Liu. LASR: Learning articulated shape reconstruction from a monocular video. In *CVPR*, 2021.
- [46] Gengshan Yang, Deqing Sun, Varun Jampani, Daniel Vlasic, Forrester Cole, Ce Liu, and Deva Ramanan. ViSER: Video-specific surface embeddings for articulated 3D shape reconstruction. 2021.
- [47] Gengshan Yang, Minh Vo, Natalia Neverova, Deva Ramanan, Andrea Vedaldi, and Hanbyul Joo. BANMo: Building animatable 3D neural models from many casual videos. In *CVPR*, pages 2853–2863, 2022.
- [48] Gengshan Yang, Shuo Yang, John Z Zhang, Zachary Manchester, and Deva Ramanan. Ppr: Physically plausible reconstruction from monocular videos. In *Proceedings of the IEEE/CVF International Conference on Computer Vision (ICCV)*, pages 3914–3924, 2023.
- [49] Chun-Han Yao, Wei-Chih Hung, Yuanzhen Li, Michael Rubinstein, Ming-Hsuan Yang, and Varun Jampani. Lassie: Learning articulated shape from sparse image ensemble via 3D part discovery. 2022.
- [50] Chun-Han Yao, Wei-Chih Hung, Yuanzhen Li, Michael Rubinstein, Ming-Hsuan Yang, and Varun Jampani. Hi-lassie: High-fidelity articulated shape and skeleton discovery from sparse image ensemble. In *CVPR*, 2023.
- [51] Chun-Han Yao, Amit Raj, Wei-Chih Hung, Yuanzhen Li, Michael Rubinstein, Ming-Hsuan Yang, and Varun Jampani. Artic3d: Learning robust articulated 3D shapes from noisy web image collections. In *Advances in Neural Information Processing Systems (NeurIPS)*, 2023. 2
- [52] Silvia Zuffi, Angjoo Kanazawa, David Jacobs, and Michael J. Black. 3D menagerie: Modeling the 3D shape and pose of animals. In *CVPR*, pages 5524–5532, 2017. 1, 2, 3